Analytic expressions for optimal inertial-confinement-fusion hohlraum wall density and wall loss

Mordecai D. Rosen* and James H. Hammer

Lawrence Livermore National Laboratory, L-039, 7000 East Avenue, Livermore, California 94551

Solutions to the radiation diffusion equation predict the absorbed energy ("wall loss") within an inertial confinement fusion (ICF) hohlraum. Comparing supersonic versus subsonic solutions suggests that a high Z metallic foam as hohlraum wall material will reduce hydrodynamic losses, and hence, net absorbed energy by $\sim 20\%$. We derive an analytic expression for the optimal density (for any given drive temperature and pulse-length) that will achieve this reduction factor and which agrees well with numerical simulations. This approach can increase the coupling efficiency of indirectly driven ICF capsules.

PACS number(s): 52.57.Bc, 52.38.Ph, 52.25.Fi, 52.25.Os

Radiation heat waves, or Marshak waves [1–3], play an important role in energy transport and in the energy balance of laser, z-pinch and heavy ion beam hohlraums for ICF and high energy density physics experiments. In these experiments, a power source, e.g., a laser, delivers energy to the interior of a high Z cavity that is converted to x-rays. Typically, most of the energy is absorbed in a thin, diffusively heated layer on the hohlraum interior surface, and reemission from that heated layer sets the radiation temperature T achieved within the hohlraum.

In our recent paper [3], (henceforward referred to as HR) we developed an analytic theory of Marshak waves via a perturbation theory using a small parameter $\varepsilon = \beta/(4+\alpha)$ where the internal energy varies as T^β and the opacity varies as $T^{-\alpha}$. A consistent theory was built up order-by-order in ε, with the benefits of good accuracy and order-by-order energy conservation. We first derived analytic solutions for supersonic Marshak waves, which remarkably allowed for arbitrary time variation of the surface temperature. We then solved the full set of subsonic equations, though specialized to the case that the surface temperature varies as t^k, where self-similar solutions can be found. Our solutions compared very well with exact analytic solutions (for the specialized cases for which they exist) and with radiation-hydrodynamic simulations.

In this paper we apply those results to the following question: Can we save on driver energy by making hohlraum walls out of low density high Z foams, which have less hydrodynamic motion (namely less radiation heated and ablated material that streams back into the hohlraum interior as a low density isothermal blow-off) and hence, reduced net absorbed energy by the walls? We answer this question using our HR analytic theory, as well as by numerical simulations. To the degree that the "pure" HR theory diverges from the simulations we derive nonideal non-self-similar corrections to the theory that bring it into agreement with the simulations. We show that low-density high Z foams can indeed bring a savings of $\sim 20\%$ in the required driver energy. Remarkably, this reduction is universal—independent of drive T and its pulse-duration τ. We derive an analytic expression

for the optimal density (for any given T and τ) that will achieve this reduction factor and which agrees very well with numerical simulations. Such an approach might allow more routine operation of the National Ignition Facility (NIF) with laser energy further away from the optics damage threshold, and still provide the nominal energy (as originally designed with solid wall hohlraums) to the fuel capsule. Reduced hydrodynamic motion of the wall material may also reduce symmetry swings, as found for heavy ion beam targets [4].

For the sake of brevity and clarity we will restrict our study here to a drive that is constant in time for a duration τ. The basic equation for supersonic, diffusive radiative transport in one dimension is

$$\rho \frac{\partial e}{\partial t} = \frac{4}{3} \frac{\partial}{\partial x} \frac{1}{K\rho} \frac{\partial \sigma T^4}{\partial x} \tag{1}$$

where e is the internal energy per unit mass, ρ is the density, T is the temperature, σ is the Stefan-Boltzmann constant, K is the Rosseland-mean opacity, t is time, and x is the spatial coordinate. e and K are specified functions of ρ, T for given materials given by $e = fT^\beta \rho^{-\mu}$ and $K^{-1} = gT^\alpha \rho^{-\lambda}$ with f, g constants. Higher density means more recombination—hence more bound electrons to provide greater line opacity; the fewer free electrons reduce the specific heat as well.

By supersonic, we mean that the velocity of the heat front is much greater than the speed of sound in the heated material. This will occur in low-density high Z foams. We consider the case of constant ρ since, in the extreme supersonic limit, hydrodynamic motion is too slow to give rise to density changes. With $\rho = $ constant, Eq. (1) gives

$$\frac{\partial}{\partial t} T^\beta = C \frac{\partial^2}{\partial x^2} T^{4+\alpha},$$

where

$$C = \frac{16}{(4+\alpha)} \frac{g\sigma}{3f\rho^{2-\mu+\lambda}}. \tag{2}$$

We introduce a dimensionless spatial variable $y = x/x_F$, where x_F is the time-dependent heat front position. In HR we solved for $T(y,t)$, for x_F, for the absorbed flux F and energy E, and then successfully compared our analytic solutions to numerical results from the radiation-hydrodynamics code
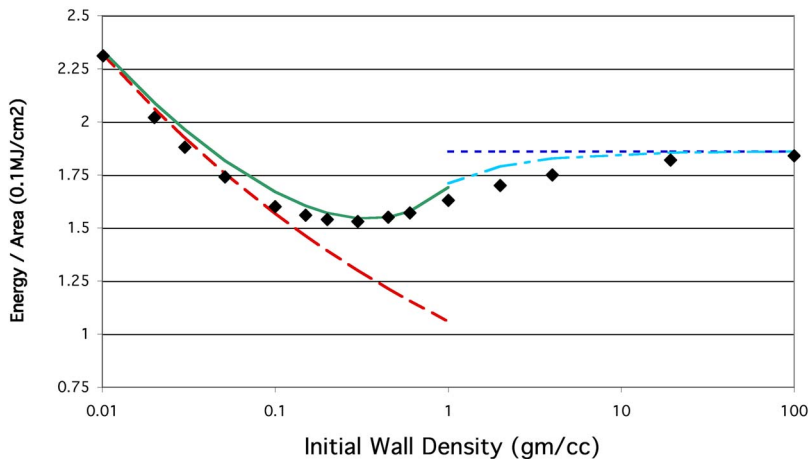
FIG. 1. (Color online) Wall loss (0.1 MJ/cm^2) vs initial wall density (g/cc). Diamond points are simulation results. Dashed line: Eq. (3). Dotted line: Eq. (5). Solid line: Eq. (6). Dot-dashed line: Eq. (7). Drive Conditions: $T=250$ eV; Duration τ: 2 ns

HYDRA [5]. For this purpose we used a fit to the opacity and equation of state for gold in the temperature range 1–3 heV (1 heV=100 eV) with temperature in heV units and ρ in g/cc: $f=3.4$ MJ/g, $\beta=1.6$, $\mu=0.14$, $g=(1/7200.)$ g/cm^2, $\alpha=1.5$, and $\lambda=0.2$. If time is in ns units, then $\sigma=1.03\times10^{-2}$ MJ/ns/cm^2. For these values, our small parameter, $\varepsilon=0.291$ and the constant C is given by $4.08\times10^{-7}/\rho^{2.06}$ cm^2/ns. For those parameters we found $x_F^2=[(2+\varepsilon)/(1-\varepsilon)]CT^{4+\alpha-\beta}\tau$, which, for our case gives $x_F(\text{cm})=0.0012\ T^{1.95}\tau^{0.5}/\rho^{1.03}$. Our solutions there led to the energy per unit area, E/A, absorbed by the gold wall:

$$E/A = 0.0029\ T^{3.55}\tau^{0.5}/\rho^{0.17}\ (\text{MJ/cm}^2)$$

$$\text{(for the pure supersonic regime).} \tag{3}$$

In HR we constructed perturbation solutions to the subsonic equations for the case that the surface temperature varies as t^k, where self-similar solutions exist. The basic equations in Lagrangian form are

$$\frac{\partial V}{\partial t} = \frac{\partial u}{\partial m}, \frac{\partial u}{\partial t} = -\frac{\partial P}{\partial m}$$

and

$$\frac{\partial e}{\partial t} + P\frac{\partial V}{\partial t} = \frac{4}{3}\frac{\partial}{\partial m}\frac{1}{K}\frac{\partial \sigma T^4}{\partial m} \tag{4}$$

where $V=1/\rho$ is the specific volume, u is the flow velocity, and P is the pressure and the mass variable $m=\int\rho dx$. The effectively infinite density at the ablation front [6–9] means that we have the boundary conditions u, V, T go to 0 at the heat front as well as $T(0,t)=T_S(t)$ at the driven surface. Our subsonic solutions included the hydrodynamic flow solution as the density changes in time and space. In the subsonic case, we again assume power-law dependence of opacity and equation of state variables as above with the additional condition that $P=re/V$. The parameter r is assumed to be of order ε (a typical value of r for gold at 1–3 heV is 0.25). Employing the self-similar ansatz, the quantity, $y=m/m_F$ with m_F the mass coordinate of the heat front, becomes the similarity variable (analogous to $y=x/x_F$ above). We again solved for $T(y,t)$, m_F, F and E, and then successfully compared our analytic solutions to numerical results from the

radiation-hydrodynamics code. Those solutions gave self-similar time dependencies for the ablated mass, $m_F(t)=m_0 T_S(t)^{1.91}t^{0.52}$ and absorbed flux $F(t)=F_0 T_S(t)^{3.35}t^{-0.41}$ with $T_S(t)=T_0 t^k$. For $k=0$, we found $m_0=9.90\cdot10^{-4}$ g/cm^2 and $F_0=3.40\cdot10^{-3}$ MJ/ns/cm^2, and thus (via a simple $E=\int Fdt$ calculation) we get

$$E/A = 0.0058\ T^{3.35}\tau^{0.59}\ (\text{MJ/cm}^2)$$

$$\text{(for the pure subsonic regime).} \tag{5}$$

Equation (5), or rather an earlier version that is quantitatively similar, has formed for several decades the basis for understanding the entire hohlraum temperature scaling experimental data base [9]. The observed scaling is well captured by a zero-dimensional model that simply compares sources (x-ray energy produced) to sinks. Typically the sinks consist of a major term: The E/A wall loss of Eq. (5) times the wall area, and a minor term of laser entrance hole (LEH) radiative losses $E/A=0.0103\ T^4\ \tau$ times the LEH area (a minor term because the LEH area is so much smaller than the wall area). Comparing Eqs. (3) and (5) we see (for a typical drive of $T=2.5$ heV and duration $\tau=2$ ns) that for densities in the neighborhood of 0.3 gm/cc there is clearly less wall loss for the supersonic case. Lowering densities further decreases opacity and increases specific heat, both in the undesirable direction of more loss to internal energy. Raising densities would be desirable as that would lower wall losses even further, but unfortunately it would take us into the subsonic regime. The sound speed, C_S, at 250 eV in gold is about 60 μm/ns, which [using the expression for x_F that precedes Eq. (3)] exceeds the supersonic heat front velocity, dx_F/dt, at 2 ns when ρ_0 is about 0.5 gm/cc.

In Fig. 1 we plot E/A versus initial ρ_0 of the wall from Eq. (3) (for $T=2.5$ and $\tau=2$.) and we plot the subsonic ("infinite density") result of Eq. (5) as well. We also plot the numerical simulation results. Note that Eq. (3) closely matches the full physics numerical simulations, deep in the supersonic regime (at very low ρ_0) when little hydrodynamic motion is expected. When hydrodynamic motion is artificially turned off in numerical simulations (not shown here), Eq. (3) closely matches those artificial simulations for all densities.

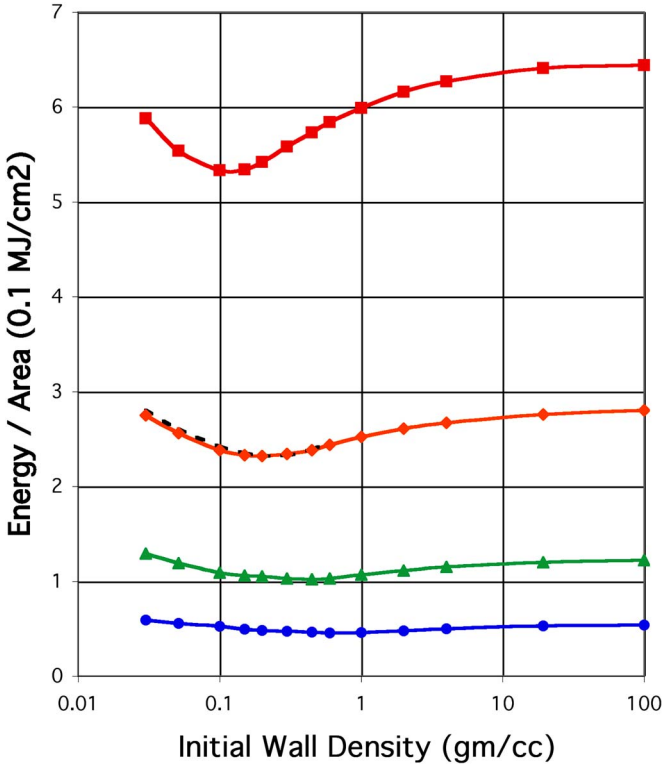To account for the divergence of the full physics simula-

FIG. 2. (Color online) Simulated wall loss (0.1 MJ/cm^2) vs initial wall density (g/cc). Drive Conditions: $T=250$ eV; Duration τ. Circles: 1/4 ns. Triangles: 1 ns. Diamonds: 4 ns. Squares: 16 ns.

tions from our self-similar solutions we reason as follows: In the supersonic regime but at higher ρ_0, rarefactions do in fact begin to eat into that portion of the heated wall nearest the drive boundary and hydro motion ensues. Consider an isothermal rarefaction wave propagating leftward (at speed C_S) into an $x<0$ half space of temperature T and original constant density ρ_0 which results in low density material blowing out, rightward. If we define $z(x,t)=1+(x/C_St)$, then the density profile is given by $\rho(x,t)=\rho_0 \exp(-z)$ and the velocity profile is given by $U(x,t)=zC_S$. Within the rarefaction the kinetic energy per unit area at any given time τ can easily be found by integrating $0.5\rho\, U^2$ over x from $-C_St$ to infinity and is equal to $\rho_0 C_S^3 \tau$. This calculates to $0.0024\rho_0^{0.79}T^{2.4}\tau(\text{MJ/cm}^2)$ and this matches the full physics simulation's opinion of the kinetic energy. Also that lower density profile within the rarefaction leads to a higher specific heat. This too can be easily found by doing a similar integral for ρe. We find that this lower density profile contributes an additional $\mu/(1-\mu)$ fraction of internal energy to that portion $(=C_S\tau/x_F)$ of the heated matter overtaken by the rarefaction front. (The portion not overtaken is still at its original density.) For our value of μ this becomes $0.0011\rho_0^{0.79}T^{2.4}\tau(\text{MJ/cm}^2)$. These two effects together now lead to a corrected E/A for the supersonic regime:

$$E/A = 0.0029\ \text{T}^{3.35}\tau^{0.5}/\rho_0^{0.17} + 0.0035\rho_0^{0.79}\text{T}^{2.4}\tau\ (\text{MJ/cm}^2)$$

(for the full supersonic regime).   (6)

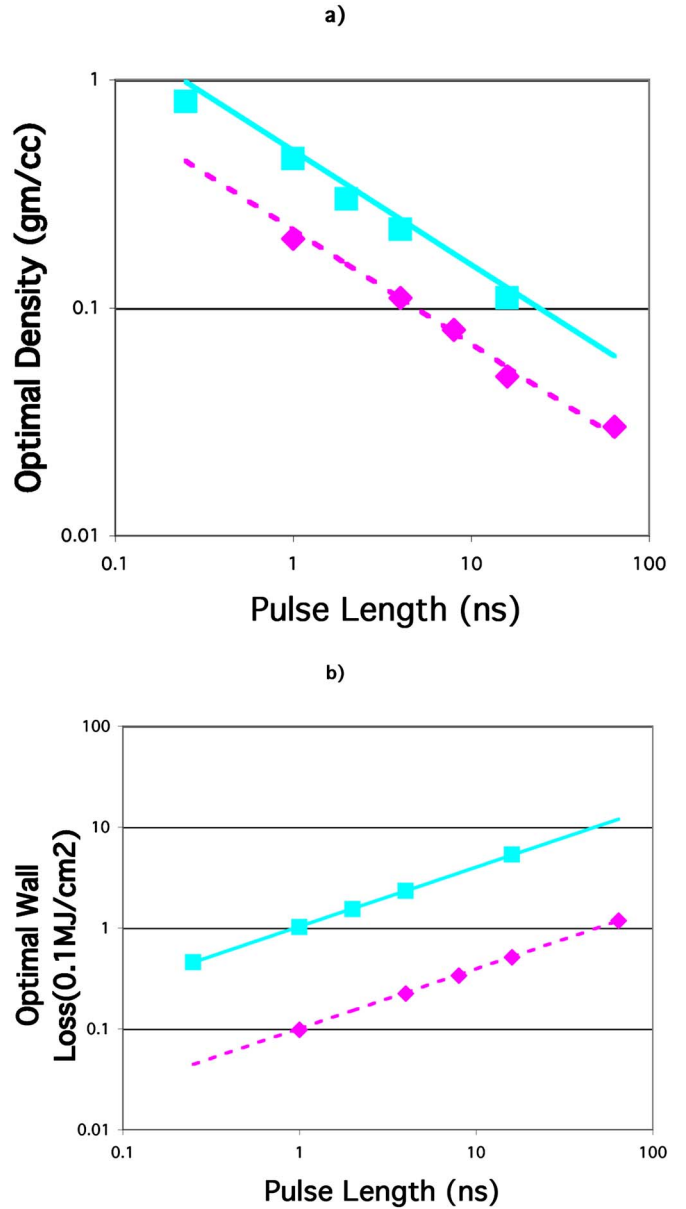The solid curve in Fig. 1 is Eq. (6) calculated out to the high

FIG. 3. (Color online) (a) Optimal density (g/cc), and (b) Optimal wall loss (0.1 MJ/cm^2), both vs pulse duration (ns). Drive conditions: $T=250$ eV: Upper solid curves: Theory [Eqs. (8a) and (8b)]. Squares: Simulations. $T=125$ eV: Lower dotted curves: Theory [Eqs. (8a) and (8b)]. Diamonds: Simulations.

ρ_0 edge of the supersonic regime and largely reproduces the E/A full physics numerical simulation curve throughout the entire supersonic regime. While these additional energy sinks reduce the full "bonus" of being supersonic that Eq. (3) naively promises, we still note a nearly 20% reduction from the solid wall result.

Note too that in Fig. 1, Eq. (5) closely matches the full physics numerical simulation at the very high end of the initial-wall-density x axis, deep in the subsonic regime. However, in the lower density part of the subsonic regime the simulations differ from the infinite density result. We believe that is due to the period of time early in the simulation when indeed the heat wave is supersonic and, therefore,
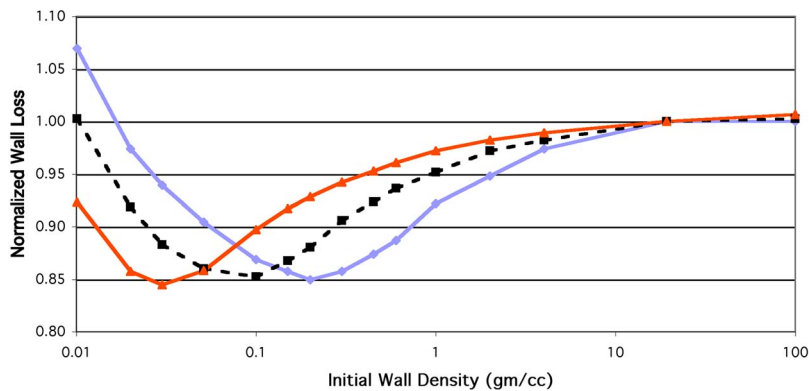
FIG. 4. (Color online) Simulated wall loss (normalized by wall loss at solid initial density) vs initial wall density (gm/cc). Drive Conditions: $T=125$ eV; Duration τ. Triangles: 64 ns. Squares: 8 ns. Diamonds: 1 ns.

less lossy. As the initial density, ρ_0, decreases, an increasingly longer early-time duration of supersonicity exists. We can correct for this by first finding $t_{catch}=0.17$ $T^{2.3}\rho_0^{-1.9}$, the time when the rarefaction front, $C_S t$, catches up to the heat front [the $x_F(t)$ that precedes Eq. (3)]. We then subtract the subsonic $E/A(t=t_{catch})$ of Eq. (5) from $E/A(\tau)$ of Eq. (5) and add in its stead the supersonic $E/A(t=t_{catch})$ of Eq. (6). For our gold parameters, the procedure outlined above leads to a simple expression for the correction:

$$E/A \text{ (MJ/cm}^2) = 0.0058 \text{ T}^{3.35}\tau^{0.59} - 0.002 \text{ T}^{4.7}/\rho_0^{1.1}$$

$$\text{(for the fullsubsonic regime).} \quad (7)$$

This result largely reproduces the E/A simulation curve throughout the entire subsonic regime, as seen in the dot-dashed curve of Fig. 1.

Since the minimum of E/A versus ρ_0 occurs at densities low enough to be within the supersonic regime, we can easily take the E/A derivative with respect to ρ_0 in Eq. (6) and find the optimal density, ρ^*:

$$\rho^* = 0.17 \text{ T}^{1.2}\tau^{-0.5}g'^{0.52}f'^{-1.04}. \quad (8a)$$

In the above we explicitly included the scaling of the opacity and specific heat coefficients (the prime denotes them being scaled to their nominal values which were given above) so that this formula can be used more generally. Plugging this back into Eq. (6) gives us the minimum E/A^*:

$$E/A^* = 0.0048 \text{ T}^{3.35}\tau^{0.59}f'^{0.68}g'^{0.41}. \quad (8b)$$

Comparing this to the E/A of the very high density (solid and above) regime of Eq. (5) we see that they scale exactly the same way. Thus their ratio implies a universal (independent of T and τ) savings of 17% when the optimal ρ^* is chosen as the initial wall density. (Also, self-consistently, ρ^* "universally" falls within the supersonic regime).

Figure 2 shows the simulation results for E/A for $T=2.5$ heV versus initial wall density, for τ varying between 0.25 and 16 ns. The shift of optimal density with τ is somewhat visible. Figure 3(a) explicitly shows the optimal densities, ρ^*, from those simulations versus τ, as well as for another set of runs at $T=1.25$ heV. They compare very well with Eq. (8a). Figure 3(b) does the same for E/A. Figure 4 shows results from the $T=1.25$ heV simulation set, wherein we plot the resultant E/A curves (normalized by their values at solid density) versus initial density, for 3 pulse lengths

varying from 1 to 64 ns. We clearly see the "universal" nature—the energy savings (versus a solid wall) at the optimal density for each τ is the same value (of about 16%), very close to our predictions.

As a final application of Eq. (8a) we consider a published design [4] of a heavy ion reactor scale hohlraum. It has been optimized via tedious full two-dimensional (2D) simulations and a foam density of 0.1 gm/cc is arrived at. It is Au-Gd and as such $g'=0.62$, $f'=1.04$, with $T=2.5$ and $t=8$, leading to our prediction of an optimal density of 0.13 gm/cc quite close to the optimized design value.

This approach should not be confused with well-known design features such as low Z gas filled hohlraums. The gas does not substantially "hold back the gold walls" and thus does not substantially save energy due to eliminating much kinetic energy. The gas merely replaces the very low density part of the isothermal high Z rarefaction (which carries very little of the total kinetic energy) with low Z gas to allow the laser to progress unimpeded (unabsorbed) to closer to the hohlraum wall for better symmetry control.

In summary, on the basis of our HR theory, as well as on the basis of numerical simulations, we have shown that hohlraum walls made of low density high Z foams can decrease wall loss by $\sim$20%. While our previous work allowed us to correctly predict the wall loss only at the two extremes of initial wall density, as shown in Fig. 1, we discovered discrepancies at intermediate densities. We were able to theoretically account for nonideal non-self similar effects in that transonic regime and thereby restore agreement with the numerical simulations therein. We derived an analytic expression, that for any T, τ allowed us to easily find a ρ^* that achieves this wall loss reduction.

Using foams may have further advantages. Reduced hydrodynamic motion of the wall material may also reduce symmetry swings, as found for heavy ion targets [2]. Detailed calculations will need to be done to further assess this aspect. More complex pulse shapes, and graded foam wall density profiles are also future work. Other effects such as "cocktail" walls [10] that have higher opacity due to a mixture of materials also calculate to save 20%. Small axial shields halfway between the fuel capsule and the laser entrance hole effectively make a hotter "inner hohlraum" [11] and also calculate to save 20% in driver energy to achieve the same capsule drive. These three 20% effects are independent of each other and are thus additive, leading perhaps to a full 50% reduction in driver energy. (There is always leakage

out the laser entrance holes that will slightly reduce these energy savings estimates.) Since the axial shield effect has already been observed [11], and initial data on cocktails [10] has already shown its promise as well, we suggests here an experiment to measure the predicted effect of lowering the hohlraum wall density. Using Eq. (8b) in the context of a simple "source=sink" model [2,9,11] implies a T higher by $0.83^{-0.3}$ or a factor of 1.06. Accounting for typical LEH losses would lower that estimate somewhat, and lead us to predict a wall that should be emitting 16% brighter—an observation well within diagnostic capabilities.

By combining all three 20% energy savings schemes, this 50% total reduction can allow NIF to operate routinely far below damage thresholds and still provide the requisite energy for experiments previously designed for full NIF energy (which is very near the damage threshold) operating with conventional hohlraums. In the longer term these effects may cut the reactor driver needs in half and thus reduce initial capital costs.

[1] R. E. Marshak, Phys. Fluids **1**, 24 (1958).
[2] M. D. Rosen, Phys. Plasmas **6**, 1690 (1999).
[3] J. H. Hammer and M. D. Rosen, Phys. Plasmas **10**, 1829 (2003).
[4] D. Callahan and M. Tabak, Phys. Plasmas **7**, 2083 (2000).
[5] M. M. Marinak *et al.*, Phys. Rev. Lett. **75**, 3677 (1995).
[6] R. Pakula and R. Sigel, Phys. Fluids **28**, 232 (1985).
[7] N. Kaiser, J. Meyer-ter-Vehn, and R. Sigel, Phys. Fluids B **1**, 1747 (1989).
[8] D. Munro, LLNL private communication (1982).
[9] M. D. Rosen, "Scaling law for radiation temperature," Laser Program Annual Report (1979), Lawrence Livermore National Laboratory, Livermore, CA, UCRL-50055–79, pp. 2–37 to 2–46 (unpublished); This work was extensively quoted and presented in J. Lindl, Phys. Plasmas **2**, 3933 (1995).
[10] T. J. Orzechowski, M. D. Rosen, H. N. Kornblum, J. L. Porter, L. J. Suter, A. R. Thiessen, and R. J. Wallace, Phys. Rev. Lett. **77**, 3545 (1996).
[11] M. D. Rosen, Phys. Plasmas **3**, 1803 (1996).